

phys. stat. sol. (a) **183**, 41 (2001)

Subject classification: 72.20.Jv; 78.47.+p; S7.14

## Radiative and Nonradiative Recombination Processes in GaN-Based Semiconductors

Y. KAWAKAMI (a), K. OMAE (a), A. KANETA (a), K. OKAMOTO (a), T. IZUMI (a),  
S. SAJOU (a), K. INOUE (a), Y. NARUKAWA (b), T. MUKAI (b), and SG. FUJITA (a)

(a) *Department of Electronic Science and Engineering, Kyoto University,  
Kyoto 606-8501, Japan*

(b) *Nitride Semiconductor Research Laboratory, Nichia Corporation, 491 Oka,  
Kaminaka, Anan, Tokushima 774-8601, Japan*

(Received October 8, 2000)

Time-resolved optical characterization is an indispensable tool to study the recombination mechanisms of excitons and/or carriers based on radiative, non-radiative, localization and many-body processes. In this paper, we review the instrumentation of various spectroscopic techniques for the assessment of  $\text{In}_x\text{Ga}_{1-x}\text{N}$ -based semiconductors such as time-resolved photoluminescence (TRPL), time-resolved electroluminescence (TREL), transient grating (TG) method to probe photothermal processes, microscopic TRPL using optical microscope, submicroscopic TRPL using scanning near field optical microscopy (SNOM) and pump-and-probe spectroscopy for the measurement of transient absorption/gain spectra. The obtained results are cited in the references.

**1. Introduction** Time-resolved spectroscopy is a useful technique to evaluate the optical properties of semiconductors. As for GaN-based semiconductors, targets as photonic devices can be classified in three subjects.

The first subject is to achieve efficient light emitting diodes (LEDs). Typical blue or green LEDs commercially available show an external quantum efficiency ( $\eta_{\text{ext}}$ ) of about 10% [1, 2]. However, further improvement of the efficiency is desired to extend the application area of LEDs, such as a replacement of light bulb or fluorescent lamp (vacuum tubes) by LEDs (solid state devices). Luminescence spectroscopy reveals that performances of LEDs at room temperature (RT) are still limited by non-radiative recombination processes, and that it should be possible to achieve  $\eta_{\text{ext}} > 40\%$  if the pathway to the non-radiative recombination centers is eliminated sufficiently. Therefore, it is very important to assess the mechanism of both radiative and non-radiative processes in order to clarify a key to get higher efficiency.

The second subject is related to the laser diodes (LDs). Since the first operation of LD has been demonstrated at 400 nm under a continuous wave (CW) mode at RT [3], the device lifetime has been made good progress, and at current stage the maximum operation time is estimated to be 10000 h [4]. However, the tuning wavelength for the stable continuous wave (CW) operation of LDs is currently in the range between 376 nm [5] and 450 nm [6], which is much narrower than that of LEDs due to the dramatic increase of  $I_{\text{th}}$  with increasing emission wavelength from 420 to 450 nm. This

---

<sup>1</sup>) Corresponding author; Tel.: +81-75-753-7573; Fax: +81-75-753-7579;  
e-mail: kawakami@kuee.kyoto-u.ac.jp

may be because internal electric field [7] is so large in In-rich active layers that the oscillator strength between electron and hole is suppressed, and/or because the optical gain cannot be generated sufficiently due to the limited number of density-of-states caused by the effect of localization [8–16]. Further breakthrough is therefore required to realize pure blue and green LDs using  $\text{In}_x\text{Ga}_{1-x}\text{N}$ -based semiconductors. Such targets can be facilitated by well-understanding the emission mechanism, as well as by the well-designing of the LD structures.

The third subject is related to the development of new photonic devices besides LEDs or LDs utilising ultrafast phenomena or optical nonlinearity.

For such purposes, it is essential to understand the recombination mechanism by assessing the dynamical behavior of excitons and/or carriers based on radiative, non-radiative, localization and many-body processes, and then to make a positive feedback to the fabrication of photonic devices.

In this paper, instrumentation of time-resolved spectroscopy developed by our group is reviewed for the assessment of recombination dynamics in  $\text{In}_x\text{Ga}_{1-x}\text{N}$ -based semiconductors.

## 2. Instrumentation of Time-Resolved Spectroscopy

**2.1 Time-resolved photoluminescence (TRPL)** Figure 1 shows the experimental apparatus for the time-resolved photoluminescence (TRPL). Pulsed photo-excitation for the TRPL is provided by the frequency doubled ( $2\omega$ ) or frequency tripled ( $3\omega$ ) beams of a mode-locked  $\text{Al}_2\text{O}_3:\text{Ti}$  laser ( $\omega$ ) which was pumped by  $\text{Ar}^+$  laser. It is possible to make a selective excitation to  $\text{In}_x\text{Ga}_{1-x}\text{N}$  active layers by using a frequency doubled beam whose tuning range is from 350 to 530 nm. Two types of pulse width, 1.5 and 100 fs can be selected by adjusting the optics in  $\text{Al}_2\text{O}_3:\text{Ti}$  laser. The pulse width of 1.5 ps is suitable

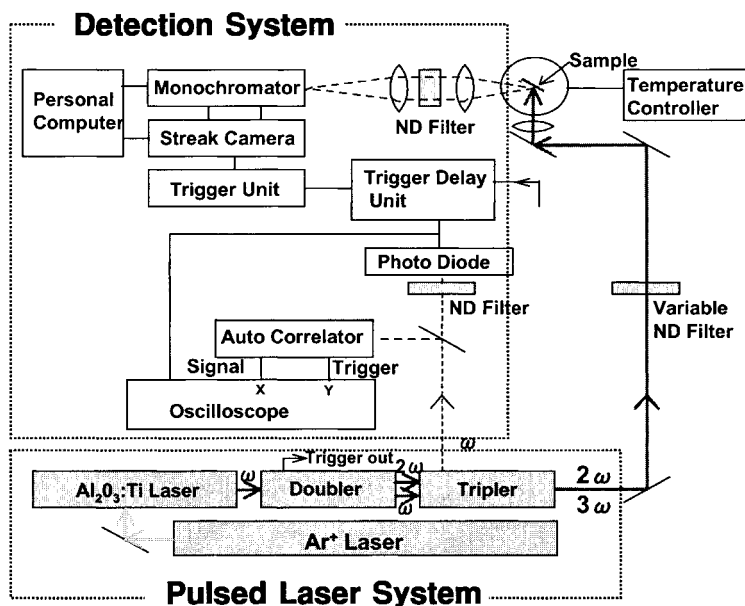


Fig. 1. Experimental apparatus for time-resolved photoluminescence

ble for the TRPL measurement if monochromaticity is needed for photoexcitation. The repetition rate of the laser is 80 MHz whose time interval is 12.5 ns. It can be reduced to 4 MHz by an acousto-optic (AO) modulator in order to avoid multi-excitation depending on the decay times. The detection is performed by means of a fast scan streak camera in conjunction with monochromator using gratings whose grooves are 100, 300 and 1200 lines/grooves. Time-resolution for the detection is about 2 ps.

The transient luminescence intensity obtained by the data of TRPL shown in Fig. 2 is generally expressed by the following equation as a function of time after excitation:

$$I(t) = I_0 \exp\left(-\frac{t}{\tau_{PL}(T)}\right), \quad (1)$$

where  $\tau_{PL}(T)$  is the decay time of luminescence at a given temperature ( $T$  in K). The inverse of  $\tau_{PL}(T)$  is the sum of three different types of transition probability,

$$\frac{1}{\tau_{PL}(T)} = \frac{1}{\tau_{rad}(T)} + \frac{1}{\tau_{non-rad}(T)} + \frac{1}{\tau_{trans}(T)}, \quad (2)$$

where  $\tau_{rad}(T)$  and  $\tau_{non-rad}(T)$  denote the radiative and non-radiative lifetimes, and  $\tau_{trans}(T)$  is the transfer time toward lower-lying energy levels. If radiative recombination occurs at the bottom of energy levels, the term of the transfer time can be neglected so that the equation is simplified as shown below.

The internal quantum efficiency ( $\eta_{int}(T)$ ) of the emission can also be written in terms of  $\tau_{rad}(T)$  and  $\tau_{non-rad}(T)$ , where

$$\frac{1}{\tau_{PL}(T)} = \frac{1}{\tau_{rad}(T)} + \frac{1}{\tau_{non-rad}(T)}, \quad \eta_{int}(T) = \frac{\tau_{non-rad}(T)}{\tau_{rad}(T) + \tau_{non-rad}(T)}. \quad (3), (4)$$

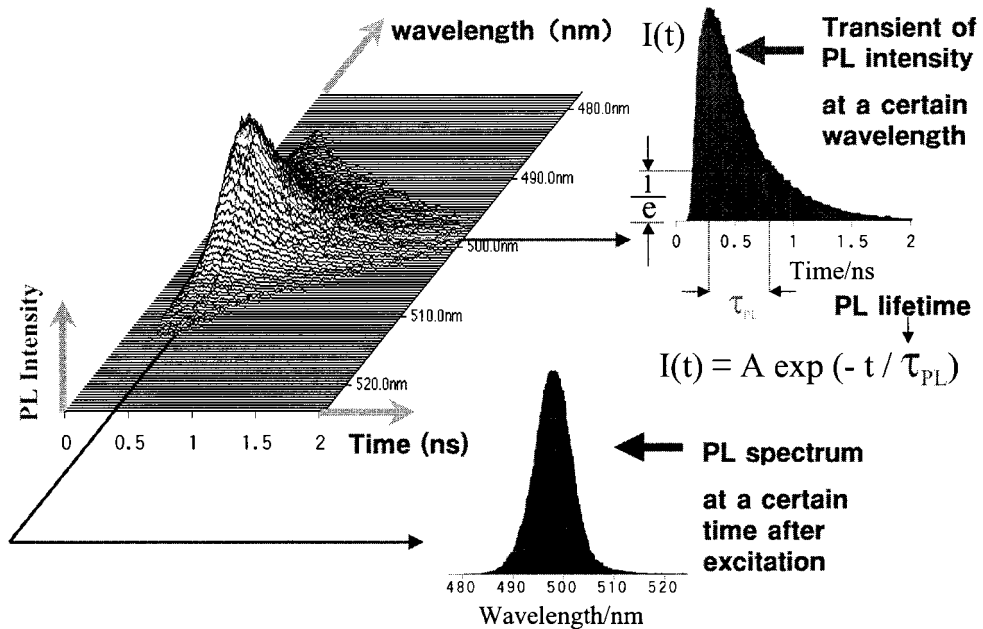


Fig. 2. Typical data obtained by time-resolved photoluminescence spectroscopy

Therefore, it is possible to estimate the temperature dependence of radiative and non-radiative lifetimes, by monitoring both  $\tau_{\text{PL}}(T)$  and  $\eta_{\text{int}}(T)$ . However, it is generally difficult to measure the  $\eta_{\text{int}}(T)$  value directly by experiment.

$\tau_{\text{non-rad}}(T)$  can be expressed by the following equation:

$$\frac{1}{\tau_{\text{non-rad}}(T)} = v_{\text{th}}\sigma N_{\text{t}}, \quad (5)$$

where  $v_{\text{th}}$ ,  $\sigma$  and  $N_{\text{t}}$  denote the thermal velocity, cross section captured to non-radiative recombination center (NRC) and the density of NRC, respectively. There is a case where the non-radiative recombination process can be ignored, if the crystal quality is relatively good (low  $N_{\text{t}}$ ) and the measurement is done at sufficiently low temperature. In fact, we sometimes see the temperature dependence of luminescence intensity  $I(T)$ , where  $I(T)$  is constant ( $I(T) = I_{\text{C}}$ ) in a low temperature region ( $T < T_{\text{C}}$ ), and then decreases gradually with increasing temperature ( $T > T_{\text{C}}$ ). In such a case, it can be assumed that internal quantum efficiency is nearly equal to unity at temperature below  $T_{\text{C}}$ , so that the luminescence decay time in this temperature range corresponds to the radiative lifetime. If necessary, validity of such an assumption can be tested by means of the detection of photothermal processes as described in Section 2.3. Then, the internal quantum efficiency can be expressed by  $\eta_{\text{int}}(T) = I(T)/I_{\text{C}}$ , and both radiative and non-radiative lifetimes at temperature above  $T_{\text{C}}$  can be given by the following equations [17]:

$$\tau_{\text{rad}}(T) = \tau_{\text{PL}}(T) \frac{I_{\text{C}}}{I(T)}, \quad (6)$$

$$\tau_{\text{non-rad}}(T) = \tau_{\text{PL}}(T) \frac{I_{\text{C}}}{I_{\text{C}} - I(T)}. \quad (7)$$

The temperature dependence of radiative lifetimes reveals the dimensionality of excitons [18, 19]. The dynamical behaviour of excitons based on localization, radiative and non-radiative recombination processes has been studied in  $\text{In}_x\text{Ga}_{1-x}\text{N}$ -based light emitting devices. It was found that excitons were weakly localized mainly due to the small fluctuation of alloy content if the In alloy content was less than about 10%. The depth of exciton localization grew with increasing In content, and the self-formation of deep localization centers was observed in the sample with  $x > 20\%$  [9, 13]. In such highly localized samples almost no temperature dependence of radiative lifetimes was observed suggesting the zero-dimensional feature of excitons [14, 15].

**2.2 Time-resolved electroluminescence (TREL)** Even if there is no short-pulse laser system, the luminescence dynamics can be assessed by applying pulsed voltage across p-i-n junction. Figure 3 shows the time-resolved electroluminescence (TREL) system [20, 21]. The pulse width and repetition rate of voltage applied to LEDs are 8 ns and 4 MHz, respectively. The condition of impedance matching can be attained with a variable resistor by minimizing the reflected current pulse monitored by a fast digital oscilloscope. Although the pulse width of applied voltage is rather broad, a time resolution of about 500 ps can be achieved by deconvoluting the current-pulse signal with the transient EL signal monitored by the streak camera. Recent progress of experimental technique has led to the TREL measurement using a pulse generator with pulse width of 150 ps.

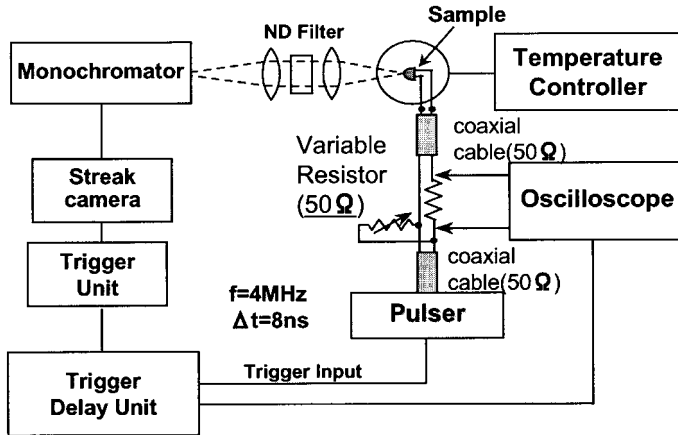


Fig. 3. Experimental apparatus for time-resolved electroluminescence

**2.3 Transient grating (TG) method to probe photothermal processes** The heat dynamics generated by non-radiative recombination processes can be assessed by measuring the photo-induced refractive index change ( $\Delta n$ ) by using the transient grating (TG) method based on third-order nonlinear spectroscopy [22–24]. The experimental set-up of the excitation and probe beams of the TG method are shown in Fig. 4. A frequency tripled beam of Nd:YAG laser (355 nm) was used for excitation. The interference pattern is created by crossing two excitation beams with an angle  $\theta$  in the sample materials. The fringe spacing  $\Lambda$  is given by

$$\Lambda = \frac{\lambda_e}{2 \sin\left(\frac{\theta}{2}\right)}. \quad (8)$$

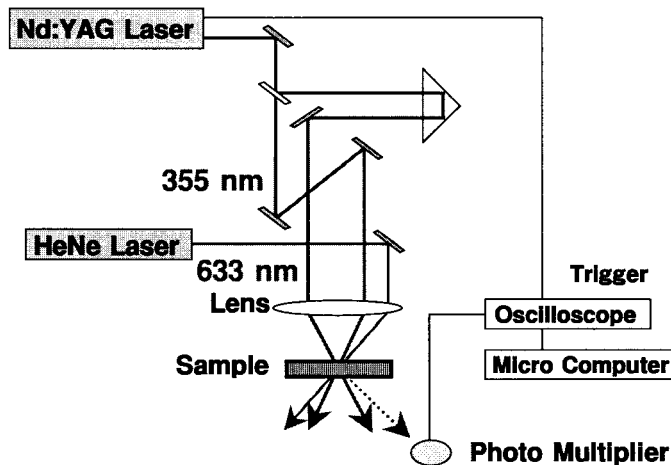


Fig. 4. Experimental apparatus for transient grating spectroscopy

Then, the light intensity in the crossing region is modulated as follows:

$$I(x) = \frac{I(1 + \cos qx)}{2}, \quad (9)$$

where  $q$  is the grating vector given by

$$q = \frac{2\pi}{\Lambda}. \quad (10)$$

The densities of carriers and/or excitons are modulated along this optical grating (population grating). The excited area releases the heat by the non-radiative recombination of carriers and/or excitons and the temperature of the sample is modulated (thermal grating). The refractive index ( $n$ ) and the absorbance ( $k$ ) of the materials are also modulated by these gratings. Such modulation of optical properties ( $\Delta n$ ,  $\Delta k$ ) are similar to the refractive grating. A probe beam from a He-Ne laser (633 nm) was partly diffracted (TG signal) by these gratings. The intensity of the TG signal can be written by

$$I_{TG} = \alpha \Delta n^2 + \beta \Delta k^2, \quad (11)$$

where  $\alpha$  and  $\beta$  are constants. The TG signal was detected by a photomultiplier tube after isolation from the probe light with a pinhole and a glass filter, recorded with a digital oscilloscope, and analyzed with a microcomputer.

**2.4 Microscopic TRPL using optical microscope** In order to assess the correlation between PL lifetimes and macroscopic dislocations, TRPL spectroscopy with micron spatial resolution [25, 26] was performed on the epitaxially laterally overgrown GaN (ELO-GaN) and  $\text{In}_x\text{Ga}_{1-x}\text{N}$  quantum wells (QWs) grown on ELO-GaN [25] by using the apparatus as shown in Fig. 5. The beam is focused down to the size of about  $1 \mu\text{m}$  using air-gapped object lens made of quartz. The fluorescence image can be observed by an optical microscope in conjunction with a CCD camera, and be detected through

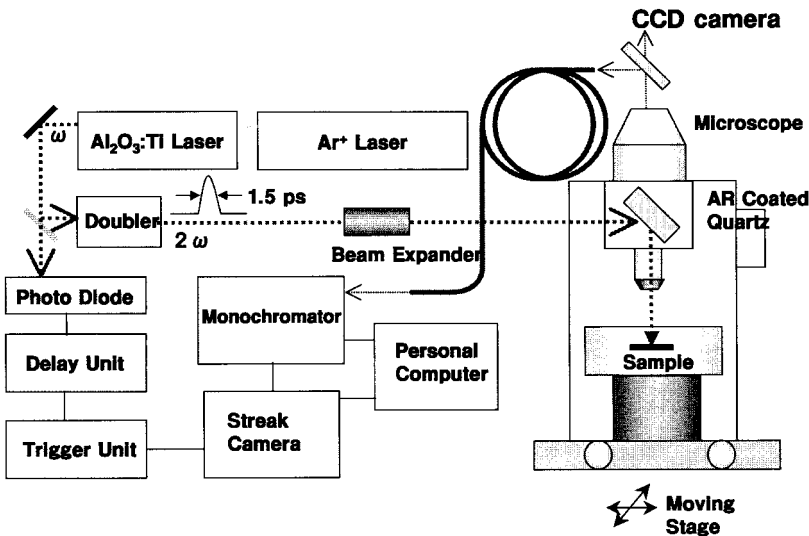


Fig. 5. Time-resolved photoluminescence with spatial resolution of about  $1 \mu\text{m}$

an UV-optical fiber in order to measure TRPL using the system shown in Fig. 1. It was found that threading dislocations act as non-radiative recombination centers, but they are not the factor to limit the internal quantum efficiency at RT [25]. The dependence of dislocation density on  $\tau_{\text{PL}}$  for  $\text{In}_x\text{Ga}_{1-x}\text{N}$  QWs became less dominant with increasing In mole fraction ( $x$  value) [27]. This result suggests that the capture cross sections of non-radiative recombination centers are greatly reduced once excitons are trapped at deep localization centers in In-rich  $\text{In}_x\text{Ga}_{1-x}\text{N}$  active layers [9].

**2.5 Submicroscopic TRPL using scanning near field optical microscopy (SNOM)** If the TRPL with nanoscopic spatial resolution could be achieved, five-dimensional (5D) data composed of space, wavelength and time would give us a more clear view on the correlation between nanoscopic structures and macroscopic optical properties. We have recently performed the first PL imaging of an  $\text{In}_x\text{Ga}_{1-x}\text{N}$ -SQW-based LED structure using scanning near field optical microscopy (SNOM) under illumination-collection mode, where photo-excitation and the PL probing are performed using the same fiber tip as shown in Fig. 6 [28].

This was achieved by tailoring the tapered structure of fiber tip composed of a pure  $\text{SiO}_2$  core to transmit UV light with low transmission loss, and to eliminate the emission background from the fiber. The measured PL mapping image revealed the variation of both peak and intensity in PL spectra according to the probing location with a resolution of about  $0.1 \mu\text{m}$ .

The variation in PL intensity observed in a yellowish green LED was from 0.8 to 1.8 (in arb. units) indicating that internal quantum efficiency fluctuates from 10% to 50% within the active layer. TRPL spectroscopy using this system is now under progress.

**2.6 Pump and probe spectroscopy for the transient absorption/gain measurement** The pump and probe spectroscopy depicted in Fig. 7 was performed for the measurements of the temporal behavior of differential absorption using a dual photo-diode array in conjunction with a 25 cm monochromator [29]. The white light used for the probe beam was generated by focusing the part of output beam from the regenerative amplifier on a  $\text{D}_2\text{O}$  cell. Detailed optical paths of both pump and probe beams are drawn in Fig. 3. The delay time of the probe beam with respect to the pump beam was tuned by changing the position of retroreflector which could be controlled by the pulse stage. Since the minimum difference in optical path was  $2 \mu\text{m}$ , a time resolution down to 6.7 fs was

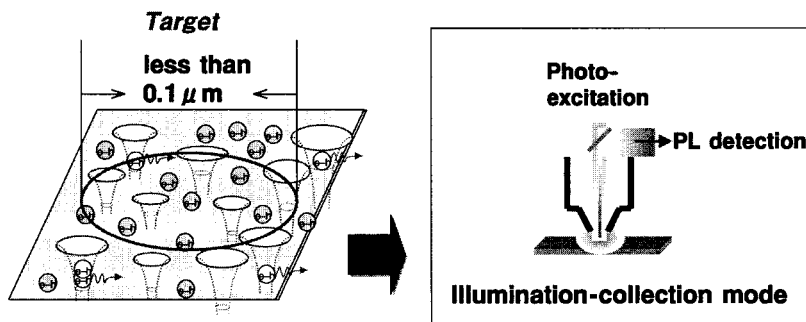


Fig. 6. An approach to improve the resolution less than  $0.1 \mu\text{m}$  by using scanning near field microscopic technique

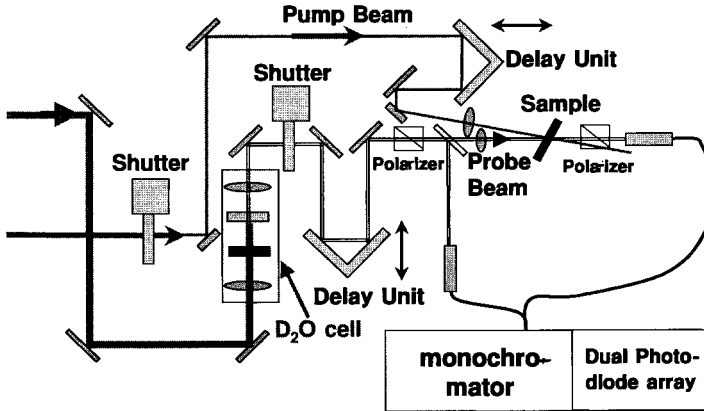


Fig. 7. Experimental set-up for the pump and probe spectroscopy

achieved. In order to detect the probe beam with spatially uniform carrier distribution in the sample, the focus size of the pump beam ( $600\ \mu\text{m}$  in diameter) was set so as to be much larger than that of the probe beam ( $200\ \mu\text{m}$  in diameter). Furthermore, the probe beam was perpendicularly polarized with respect to the pump beam, and the transmitted probe beam polarized in this direction was detected to avoid scattering of the pump beam.

In the pump and probe spectroscopy, the transmission spectrum of the probe beam detected in the presence of the pump beam ( $T + \Delta T$ ) is compared to the spectrum without pump beam ( $T$ ), giving the frequency ( $\omega$ )-dependent  $\Delta T(\omega, I_{\text{ex}}, t_d)$  of the sample for different intensities of the pump ( $I_{\text{ex}}$ ), and for different time delays after the pulse pumping ( $t_d$ ). The photo-induced change of optical density ( $\Delta OD(\omega, I_{\text{ex}}, t_d)$ ) is expressed by the following equation:

$$\Delta OD = \log \left( \frac{T}{T + \Delta T} \right) = 0.434 \Delta \alpha d, \quad (12)$$

where  $\Delta \alpha(\omega, I_{\text{ex}}, t_d)$  is the photo-induced change of absorption coefficient,  $d$  is the thickness of absorbing layer. A schematic of  $\alpha$  and  $\alpha + \Delta \alpha$  is illustrated in Fig. 8. In

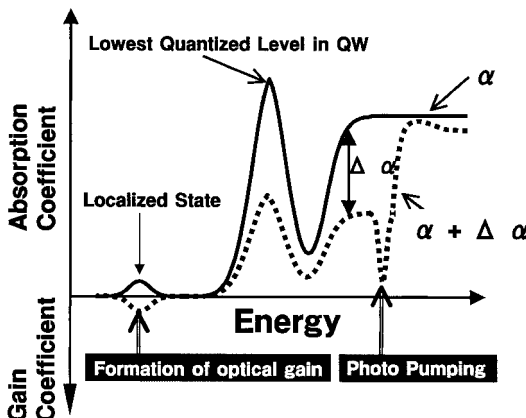


Fig. 8. Schematic of carrier dynamics in a localized system.  $\alpha$  and  $\alpha + \Delta \alpha$  denote absorption coefficient under low photoexcitation and under photo pumping, respectively

normal case, photo-bleaching ( $\alpha + \Delta\alpha < \alpha$ ) is observed because of the state-filling of photo-induced carrier, and  $\alpha + \Delta\alpha$  becomes negative, giving rise to optical gain if population inversion is achieved. As can be observed in the modulation spectroscopy such as photoreflectance (PR) or electroreflectance (ER), it is likely that the  $\Delta OD$  signal would not be affected by the interference of transmittance because of the cancellation between the denominator and numerator in Eq. (1). However, interference oscillation was observed probably because of the change of refractive index induced by photo-excitation. Therefore, it was necessary to reduce the internal reflection of the probe beam by means of the Brewster angle of incidence (about  $70^\circ$ ) with p-polarization.

Dynamical behavior of optical gain formation has been assessed at RT in the  $\text{In}_x\text{Ga}_{1-x}\text{N}$  multi-quantum-well (MQW)-based LD structures by employing pump and probe spectroscopy with a pulse width of 150 fs. The LDs are composed of a)  $\text{In}_{0.1}\text{Ga}_{0.9}\text{N}$ – $\text{In}_{0.02}\text{Ga}_{0.98}\text{N}$  MQW and b)  $\text{In}_{0.3}\text{Ga}_{0.7}\text{N}$ – $\text{In}_{0.05}\text{Ga}_{0.95}\text{N}$  MQW, whose stimulated emissions correspond to near ultraviolet (390 nm) and blue (440 nm), respectively. The optical gain was contributed from the nearly delocalized states (the lowest-quantized MQW levels (LQL)) in the sample a, while it was from highly localized levels with respect to LQL by 500 meV for the sample b. It was found that the photo-generated carriers rapidly (less than 1 ps) transferred to LQL, and then relaxed to the localized tail within the time scale of about 5 ps, giving rise to the optical gain. Such gain spectra were saturated and other bands appeared in the vicinity of LQL under higher photo-excitation [30].

**Acknowledgements** The authors are grateful for the financial support of the Grant-in-Aid for Scientific Research from the Ministry of Education, Science, Sports and Culture. A part of this work was performed using the facility at the Venture Business Laboratory in Kyoto University (KU-VBL).

## References

- [1] S. NAKAMURA, M. SENOH, N. IWASA, S. NAGAHAMA, T. YAMADA, and T. MUKAI, *Jpn. J. Appl. Phys.* **34**, L1332 (1995).
- [2] S. NAKAMURA, M. SENOH, N. IWASA, S. NAGAHAMA, T. YAMADA, and T. MUKAI, *Jpn. J. Appl. Phys.* **37**, L479 (1998).
- [3] S. NAKAMURA, M. SENOH, S. NAGAHAMA, N. IWASA, T. YAMADA, T. MATSUSHITA, H. KIYOKU, and Y. SUGIMOTO, *Jpn. J. Appl. Phys.* **35**, L74 (1996).
- [4] S. NAKAMURA, M. SENOH, S. NAGAHAMA, T. MATSUSHITA, H. KIYOKU, Y. SUGIMOTO, T. KOZAKI, H. UMEMOTO, M. SANO, and T. MUKAI, *Jpn. J. Appl. Phys.* **38**, L226 (1999).
- [5] I. AKASAKI, H. AMANO, S. SOTA, H. SAKAI, T. TANAKA, and M. KOIKE, *Electron. Lett.* **32**, 1105 (1996).
- [6] S. NAKAMURA, M. SENOH, S. NAGAHAMA, N. IWASA, T. MATSUSHITA, and T. MUKAI, *Appl. Phys. Lett.* **76**, 22 (2000).
- [7] T. TAKEUCHI, C. WETZEL, S. YAMAGUCHI, H. SAKAI, H. AMANO, I. AKASAKI, Y. KANEKO, S. NAKAGAWA, Y. YAMAOKA, and N. YAMADA, *Appl. Phys. Lett.* **73**, 1691 (1998).
- [8] S. CHICHIBU, T. AZUHATA, T. SOTA, and S. NAKAMURA, *Appl. Phys. Lett.* **69**, 4188 (1996).
- [9] Y. NARUKAWA, Y. KAWAKAMI, M. FUNATO, SZ. FUJITA, SG. FUJITA, and S. NAKAMURA, *Appl. Phys. Lett.* **70**, 868 (1997).
- [10] Y. NARUKAWA, Y. KAWAKAMI, SG. FUJITA, and S. NAKAMURA, *phys. stat. sol. (a)* **176**, 39 (1999).
- [11] T. DEGUCHI, T. AZUHATA, T. SOTA, S. CHICHIBU, and S. NAKAMURA, *Mater. Sci. Engng. B* **50**, 251 (1997).
- [12] A. SATAKE, Y. MASUMOTO, T. MIYAJIMA, T. ASATSUMA, and M. IKEDA, *Phys. Rev. B* **60**, 16660 (1999).

- [13] Y. NARUKAWA, Y. KAWAKAMI, SZ. FUJITA, SG. FUJITA, and S. NAKAMURA, *Phys. Rev. B* **55**, R1938 (1997).
- [14] Y. NARUKAWA, Y. KAWAKAMI, SG. FUJITA, and S. NAKAMURA, *Phys. Rev. B* **59**, 10283 (1999).
- [15] Y. KAWAKAMI, Y. NARUKAWA, K. OMAE, SG. FUJITA, and S. NAKAMURA, *phys. stat. sol. (a)* **178**, 331 (2000).
- [16] Y. CHO, T. J. SCHMIDT, S. BIDNYK, G. H. GAINER, J. J. SONG, S. KELLER, U. K. MISHRA, and S. P. DENBAARS, *Phys. Rev. B* **61**, 7571 (2000).
- [17] R. C. MILLER, D. A. KLEINMAN, W. A. NORDRAND, JR., and A. C. GOSSARD, *Phys. Rev. B* **22**, 863 (1980).
- [18] P. LEFEBVRE, J. ALLÈGRE, B. GIL, A. KAVOKIN, H. MATHIEU, W. KIM, A. SALVADOR, A. BOTCHKAREV, and H. MORKOÇ, *Phys. Rev. B* **57**, R9447 (1998).
- [19] Y. NARUKAWA, S. SAIJOU, Y. KAWAKAMI, SG. FUJITA, T. MUKAI, and S. NAKAMURA, *Appl. Phys. Lett.* **74**, 558 (1999).
- [20] Y. NARUKAWA, S. SAIJOU, Y. KAWAKAMI, SZ. FUJITA, SG. FUJITA, and S. NAKAMURA, *J. Cryst. Growth* **189/190**, 593 (1998).
- [21] Y. KAWAKAMI, Y. NARUKAWA, K. SAWADA, S. SAIJOU, SZ. FUJITA, SG. FUJITA, and S. NAKAMURA, *Mater. Sci. Engng. B* **50**, 256 (1997).
- [22] H. HAAG, B. HÖNERLAGE, O. BRIOT, and R. L. AULOMBARD, *Phys. Rev. B* **60**, 11624 (1999).
- [23] K. OKAMOTO, Y. KAWAKAMI, SG. FUJITA, and M. TERAZIMA, *Anal. Sci.*, in press.
- [24] K. OKAMOTO, Y. KAWAKAMI, SG. FUJITA, M. TERAZIMA, and S. NAKAMURA, *Jpn. J. Appl. Phys.*, in press.
- [25] T. IZUMI, Y. NARUKAWA, K. OKAMOTO, Y. KAWAKAMI, SG. FUJITA, and S. NAKAMURA, *J. Lum.* **87/89**, 1196 (2000).
- [26] K. OKAMOTO, H. C. KO, Y. KAWAKAMI, and SG. FUJITA, *J. Cryst. Growth* **214/215**, 639 (2000).
- [27] T. IZUMI, K. INOUE, Y. NARUKAWA, K. OKAMOTO, Y. KAWAKAMI, SG. FUJITA, A. TSUJIMURA, I. KIDOGUCHI, and Y. BAN, *Jpn. J. Appl. Phys.*, in press.
- [28] A. KANETA, T. IZUMI, K. OKAMOTO, Y. KAWAKAMI, SG. FUJITA, Y. NARITA, T. INOUE, and T. MUKAI, *Jpn. J. Appl. Phys.*, in press.
- [29] Y. NARUKAWA, Ph.D. Thesis, Kyoto University, 2000.
- [30] Y. KAWAKAMI, Y. NARUKAWA, K. OMAE, S. NAKAMURA, and SG. FUJITA, *Appl. Phys. Lett.* **77**, 2151 (2000).